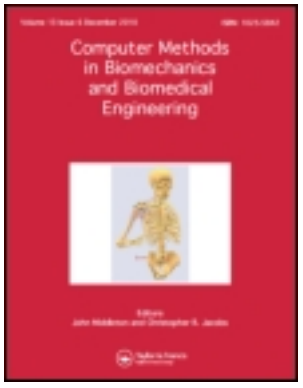

Computer Methods in Biomechanics and Biomedical Engineering

Publication details, including instructions for authors and subscription information:
http://www.tandfonline.com/loi/gcmb20

Mixed-mode loading of the cement-bone interface: a finite element study

Daan Waanders [a], Dennis Janssen [a], Katia Bertoldi [b c], Kenneth A. Mann [d] & Nico Verdonschot [a e]

[a] Orthopaedic Research Laboratory, Radboud University Nijmegen Medical Centre, P.O. Box 9101, 6500 HB, Nijmegen, The Netherlands

[b] School of Engineering and Applied Sciences, Harvard University, 29 Oxford Street, Cambridge, MA, 02138, USA

[c] Department of Multi Scale Mechanics, University of Twente, P.O. Box 217, 7500 AE, Enschede, The Netherlands

[d] Department of Orthopaedic Surgery, Institute For Human Performance, SUNY Upstate Medical University, 750 East Adams Street, Syracuse, NY, 13210, USA

[e] Laboratory for Biomechanical Engineering, University of Twente, P.O. Box 217, 7500 AE, Enschede, The Netherlands

Available online: 17 Dec 2010

To cite this article: Daan Waanders, Dennis Janssen , Katia Bertoldi , Kenneth A. Mann & Nico Verdonschot (2011): Mixed-mode loading of the cement-bone interface: a finite element study, Computer Methods in Biomechanics and Biomedical Engineering, 14:02, 145-155

To link to this article: http://dx.doi.org/10.1080/10255842.2010.535814

Computer Methods in Biomechanics and Biomedical Engineering
Vol. 14, No. 2, February 2011, 145–155

Taylor & Francis
Taylor & Francis Group

Mixed-mode loading of the cement–bone interface: a finite element study

Daan Waanders[a]*, Dennis Janssen[a1], Katia Bertoldi[b,c2,3], Kenneth A. Mann[d4] and Nico Verdonschot[a,e5,6]

[a]*Orthopaedic Research Laboratory, Radboud University Nijmegen Medical Centre, P.O. Box 9101, 6500 HB Nijmegen, The Netherlands;* [b]*School of Engineering and Applied Sciences, Harvard University, 29 Oxford Street, Cambridge, MA 02138, USA;* [c]*Department of Multi Scale Mechanics, University of Twente, P.O. Box 217, 7500 AE Enschede, The Netherlands;* [d]*Department of Orthopaedic Surgery, Institute For Human Performance, SUNY Upstate Medical University, 750 East Adams Street, Syracuse, NY 13210, USA;* [e]*Laboratory for Biomechanical Engineering, University of Twente, P.O. Box 217, 7500 AE Enschede, The Netherlands*

(*Received 17 May 2010; final version received 26 October 2010*)

While including the cement–bone interface of complete cemented hip reconstructions is crucial to correctly capture their response, its modelling is often overly simplified. In this study, the mechanical mixed-mode response of the cement–bone interface is investigated, taking into account the effects of the well-defined microstructure that characterises the interface. Computed tomography-based plain strain finite element analyses models of the cement–bone interface are built and loaded in multiple directions. Periodic boundaries are considered and the failure of the cement and bone fractions by cracking of the bulk components are included. The results compare favourably with experimental observations. Surprisingly, the analyses reveal that under shear loading no failure occurs and considerable normal compression is generated to prevent interface dilation. Reaction forces, crack patterns and stress fields provide more insight into the mixed-mode failure process. Moreover, the cement–bone interface analyses provide details which can serve as a basis for the development of a cohesive law.

Keywords: finite element; bone; bone cement; interface

Introduction

In finite element analyses (FEA) of complete cemented total hip reconstructions, the mechanical response of the cement–bone interface is often overly simplified. In previous analyses, the cement–bone interface was uniformly modelled as infinitely stiff (Katoozian and Davy 2000; Hung et al. 2004; Stolk et al. 2007), as a layer of soft tissue elements (Verdonschot and Huiskes 1997; Colombi 2002) and as a frictional contact layer (Lewis and Duggineni 2006). However, experiments with laboratory prepared cement–bone interface specimens demonstrate that the variety of the interfacial microstructure leads to a substantial variance in its mechanical compliance and strength (Mann et al. 2008). Moreover, post-mortem retrievals show that the cement–bone interface is considerably degenerated making the interface even more compliant (Bishop et al. 2009; Miller et al. 2010; Race et al. 2010).

Micro-mechanical FEA models have recently been developed, which are able to reproduce the static and fatigue behaviour of the cement–bone interface *in vitro* (Janssen et al. 2008, 2009; Waanders et al. 2009, 2010). However, such micro models cannot be implemented in complete FEA models of hip reconstructions due to their extremely large computational cost.

Cohesive zone models have attracted a growing interest in the scientific community to model the cement–bone interface in complete hip reconstructions (Mann and Damron 2002; Moreo et al. 2006, 2007; Perez et al. 2009). In cohesive zone models, a constitutive relation, or cohesive zone law, between the traction and opening displacement in both normal and tangential direction has to be defined. Moreover, the response of the interface to mixed-mode loading may be captured either by implementing an independent traction-opening displacement relationships in normal and tangential direction (Mann and Damron 2002) or defining a mixed-mode model with an interaction between normal and tangential opening displacements (Moreo et al. 2006, 2007; Perez et al. 2009). The responses of such mixed-mode models can be fit to mixed-mode experimental observations (Mann et al. 2001; Wang et al. 2010). However, a major limitation of these mixed-mode experiments is the wide range in mechanical responses as a result of specimen variety, since destructive mechanical testing in multiple directions with a single cement–bone interface specimen is not possible.

Several studies have focused on the relation between the mechanical response of the cement–bone interface and its interfacial morphology under tensile loading. It was shown that the tensile strength of the interface is strongly

*Corresponding author. Email: d.waanders@orthop.umcn.nl

ISSN 1025-5842 print/ISSN 1476-8259 online

DOI: 10.1080/10255842.2010.535814
http://www.informaworld.com

related to the mineral density of the cement–bone interface obtained from quantitative computed tomography (CT) and the maximum cement penetration in the bone (Lotz et al. 1991; Mann et al. 1997). Moreover, unidirectional experiments and FEA analyses have successfully related the strength and stiffness of the cement–bone interface to the contact area between the bone and cement (Mann et al. 2008), the average level of cement penetration into the bone (Waanders et al. 2010) and the fraction of cement–bone intersections over the complete interface (Miller et al. 2010). However, no reports have been made to explore the relationship between strength of the interface and its morphology under different mixed loading conditions.

The goal of this study was to investigate in detail the mechanical mixed-mode response of the cement–bone interface. The acquired results, in terms of tractions and displacements, should subsequently serve as a basis for the implementation in cohesive elements. Using a multi-scale approach, CT-based FEA models of the cement–bone interface were built and tested, under loading in multiple directions. The model accounted for the failure of both the cement and bone by cracking of the bulk components. We focused our analysis on the following key-aspects: (1) the relationship between the normal and tangential tractions during mixed-mode loading of the cement–bone interface and (2) the relation between the interfacial response and morphology under mixed-mode loading.

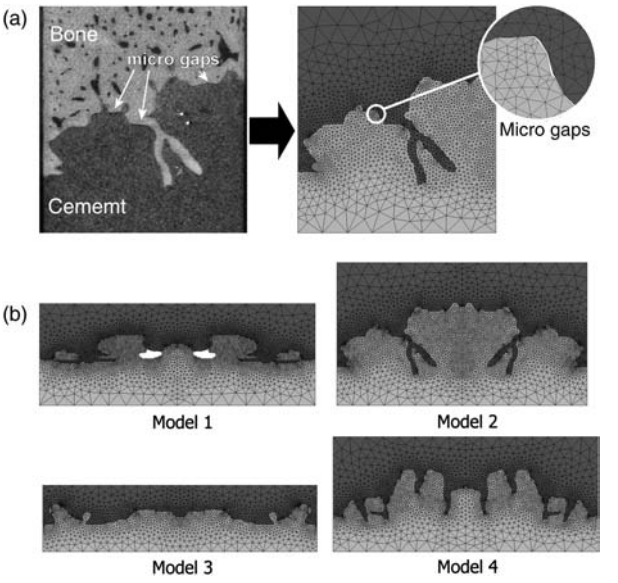

Figure 1. (a) Out of one slice of the micro-CT data of the cement–bone interface, the generalised plain strain model was created. The micro-CT data contained only one bone and one cement body to avoid any redundant particles. Micro gaps between the bone and the cement were recreated using a custom algorithm (Waanders et al. 2009). (b) All models were mirrored what resulted in four models with distinct differences in dimensions and interface morphology (Table 1). The four mirrored models had an average width, 'w' and thickness, 't', of 9.43 and 3.80 mm, respectively.

Methods

Four generalised two-dimensional (2D) plane strain FEA models of the cement–bone interface were built, based on a single micro-CT slice (12 μm isotropic resolution, see Figure 1(a)) of four different physical specimens containing the cement–bone interface (Waanders et al. 2009). The selected slices contained only one bone and cement body to avoid floating particles. The FEA models included the complex morphology of the cement–bone interface and were meshed using a custom algorithm to recreate the gaps between the cement and bone (Waanders et al. 2009). The top edge of the bone and bottom edge of the cement had an offset of ~1 mm relative to the contact interface to avoid mechanical boundary artefacts at the contact interface, since previous studies have shown that the majority of motion takes place at the contact interface and not in the surrounding materials (Mann et al. 2008, 2009; Waanders et al. 2009; Yang et al. 2010). Each model was mirrored to fulfil the periodic boundary conditions (Mullins et al. 2007; Pahr and Zysset 2008); this will be clarified later (Figure 1(b)). The accuracy of the mesh was ascertained through a mesh refinement study and the resulting models contained on average 96,900 elements and 23,400 nodes. Contact between the bone and cement was modelled using a double-sided node to surface contact algorithm (MSC.MARC 2007r1, MSC Software Corporation, Santa Ana, CA, USA) with a friction coefficient of 0.3 (Janssen et al. 2008).

Both the bone and the cement were initially modelled as isotropic linear elastic materials. Young's modulus (E) and Poisson's ratio (ν) of the cement were taken as 3000 MPa and 0.3, respectively (Harper and Bonfield 2000; Janssen et al. 2009). The bone properties were based upon micro-CT greyscale values, which were converted to equivalent hydroxyapatite (HA)-densities using a calibration phantom. The assumption of a linear relationship between HA-density and Young's modulus (Lotz et al. 1991) resulted in Young's modulus' $0.1 \leq E \leq 20{,}000$ MPa ($\nu = 0.3$).

Previous experiments showed the formation of cracks in the cement and bone when loaded to failure (Mann et al. 2008). Crack formation in the bulk bone and cement due to excessive stresses was included in the models using an adapted custom-written FEA algorithm to simulate static failure (Stolk et al. 2004). Static failure occurred when the local principal tensile stress either in the cement or in the bone exceeded the strength of the material. The strength of the cement was taken as 40 MPa (Lewis 1997; Harper and Bonfield 2000), while the strength of the bone was based on the local Young's modulus (Keyak et al. 2005;

Waanders et al. 2010).

$$S = 102\left(\frac{E}{14,900}\right)^{(1.80/1.86)}.$$

Cracks were simulated by setting Young's modulus in the direction perpendicular to the corresponding principal stress direction to 0.1 MPa.

Periodic boundary conditions were applied to both sides of the model in order to establish a multi-scale representation of the cement–bone interface. In this way, the complete cement–bone interface was considered as a series of periodic micro structures (Kadir et al. 2010). The periodic boundary conditions were implemented constructing nodal links between nodes periodically located on the left and right side of the model (Figure 2(a); Salomonsson and Andersson 2008).

$$u_x(0, y) = u_x(w, y) \quad u_y(0, y) = u_y(w, y).$$

In these two equations, 'u_i' represents the displacement and 'w' the width. To avoid bone-to-cement nodes at the boundary between two different periodic cells, the models were mirrored. Moreover, all nodes of the bottom edge were fixed in both directions (Figure 2(b)), while the nodes on the top edge uniformly displaced.

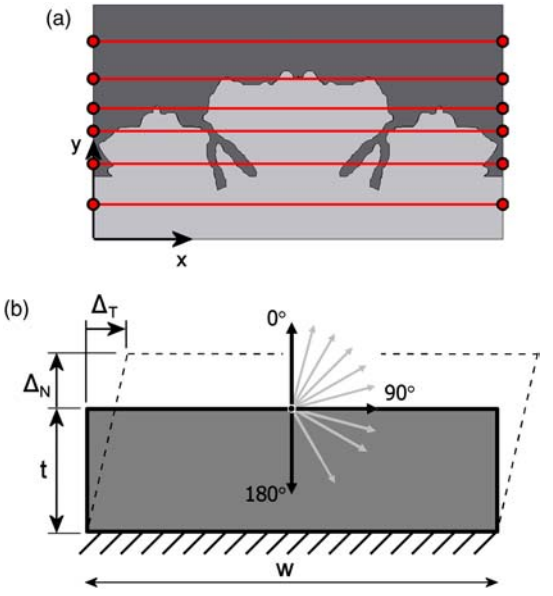

Figure 2. (a) Periodic boundary conditions were applied to the left and right side of each model by applying links between each side. As a result of the mirroring of the models, only bone-to-bone and cement-to-cement links were created. Moreover, this subsequently resulted in a smooth '*infinite*' contour of the contact interface between the bone and cement. (b) The bottom part of each model was fixated in x- as well as y-direction. The periodic boundary description resulted in equal motion of the nodes on the model's left and right side: $u_x(0, y) = u_x(w, y)$, $u_y(0, y) = u_y(w, y)$. The nodes in top plane ($y = t$) were incrementally displaced under 11 different angles, α. Tangential displacements were consequently applied in positive x-direction.

Each model was loaded until failure by applying an incremental displacement ($\Delta = 0.001$ mm) to the top edge. Eleven directions (α) were considered: 0° (pure tension), 15°, 30°, 45°, 60°, 75°, 90° (pure shear), 105°, 120°, 150°and 180° (pure compression) (Figure 2(b)). Hence, the incremental normal and tangential displacement, Δ_N and Δ_T, applied to the nodes on the top edge were

$$\Delta_N = \Delta\cos(\alpha) \quad \Delta_T = \Delta\sin(\alpha).$$

The resultant reaction force was calculated as well as its normal (T_N) and tangential (T_T) component.

The interface morphology was quantified using a CT-based stereology approach (Miller et al. 2010; Waanders et al. 2010). A 12 × 6 grid was spanned over the micro-CT scan of each model (Figure 3). For each of the 12 vertical and 6 horizontal lines, the local normal and tangential cement interdigitation was measured, respectively. Local cement interdigitation was defined as the total amount of cement that was captured between two pieces of bone for the grid line. Subsequently, the average interdigitation was determined for both normal (int_N) and tangential direction, (int_T). The tangential interdigitation was doubled to account for the interdigitation for the mirrored models. The average interdigitation in each direction was used as a global measure of cement penetration. Subsequently, for each loading angle (α), the average normal and tangential interdigitation was determined as

$$int_{N,\alpha} = |int_N\cos(\alpha)| \quad int_{T,\alpha} = int_T\sin(\alpha).$$

The influence of the choice of an ~1 mm offset dimension was explored by extending the cement and bone an additional 1 mm from the cement–bone interface

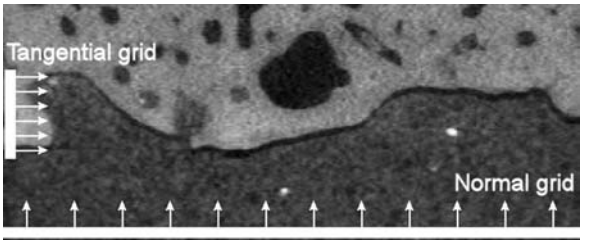

Figure 3. A grid was superimposed over each specimen. Twelve vertical lines were subdivided over the complete specimen's width with equal spacing. For each line, the local interdigitation was determined (Miller et al. 2010; Waanders et al. 2010). The 12 local interdigitations were averaged resulting in the average normal interdigitation, int_N, (Table 1). A similar approach was used to determine the cement interdigitation in tangential direction, int_T. The only difference was that the six horizontal lines were spanned over the height of interdigitation and not the specimen's complete height and that the tangential interdigitation was subsequently doubled.

in model 2. The extended model 2 was subsequently loaded in pure tension (0°) and pure shear (90°) and the results, were compared with the original model 2.

During each simulation, the normal (T_N) and tangential tractions (T_T) as well as the normal (Δ_N) and tangential displacements (Δ_T) were monitored. For each simulation, four traction–displacement ($T - \Delta$) responses were analysed: $T_N - \Delta_N$, $T_N - \Delta_T$, $T_T - \Delta_T$ and $T_T - \Delta_N$. In normal and tangential direction, the initial stiffness (($\partial T_N/\partial \Delta_N$) and ($\partial T_T/\partial \Delta_T$)) and strength ($T_{N,ult}$ and $T_{T,ult}$) were determined. Linear regression analysis was used to determine relationships between the normalised cement interdigitation, $int_{N,\alpha}$ and $int_{T,\alpha}$, and interface initial stiffness and strength.

Results

All four models showed similar response under mixed-mode loading. In pure tension ($\alpha = 0°$), the cement–bone interface showed a traction–displacement response with an initial stiffness followed by initiation of damage and softening (Figure 4(a)). Moreover, under pure tension–the tractions in the tangential direction (T_T) were found to be negligible (Figure 4(d)). Symmetric crack patterns were characterised in breaking off bone and cement spurs (Figure 5). The ultimate strengths ($T_{N,ult}$) in pure tension for the four models ranged from 1.28 to 2.79 MPa and the normal stiffness ($\partial T_N/\partial \Delta_N$) from 123 to 251 MPa/mm (Table 1). In contrast, pure compressive loading ($\alpha = 180°$) resulted in a linear $T_N - \Delta_N$ relationship (Figure 4(a)), with stiffness ranging from 769 to 1538 MPa/mm (Table 1). Hardly any cracks occurred in pure compression (Figure 5).

In pure shear ($\alpha = 90°$), a linear increase of T_T as a function Δ_T was found; and none of the models reached failure (Figure 4(c)). The tangential stiffness ($\partial T_T/\partial \Delta_T$) ranged from 222 to 332 MPa/mm for all the models. Surprisingly, despite the lack of a softening phase in pure shear, cracks were observed which originated at the contact interface and progressed into the bone and cement bulk without breaking off spurs (Figure 5). Additionally, a considerable compressive traction was observed to prevent dilation of the interface (Figure 4(b)).

For all the considered intermediate values of α a smooth transition between responses described above was observed (Figures 4 and 6). It is interesting to observe that for $\alpha = 45°$, 60° and 75° the normal tractions become eventually compressive. To better understand this counter intuitive response, we focused on model 3 where for $\alpha = 45°$ the stress distribution at different points along the loading path was reported (Figure 7). We observed that for this value of α, the $T_N - \Delta_N$ response increased linearly until the ultimate strength ($T_{N,ult}$) was reached. At this point, all bone reaction forces acted in positive y-direction and few cracks were observed (Figure 7(a)). Nearly the whole stress field in normal direction (σ_{yy}) was positive and the stress field in tangential direction (σ_{xx}) revealed the first areas subjected to compression due to the bone–cement contact. After this point, T_N decreased and when $T_N = 0$ both tensile and compressive contact forces were observed (Figure 7(b)). Cracks were present in both bone and cement and progressed into the bulk materials. Positive and negative values were found for the stress field σ_{yy}. The stress field σ_{xx} showed some areas of compression which were located between the contact area and the originated cracks. When displaced further, T_N became negative, so that normal compression was induced even with the positive normal displacement. When $T_N = -T_{N,ult}$, almost all reaction forces acted in the negative y-direction (Figure 7(c)). The amount of cracks increased considerably and almost the whole area with bone–cement interlock was loaded in compression, σ_{xx}.

Comparison of all mixed-mode responses showed that the normal traction (T_N) and displacements (Δ_N) at which the normal strength was reached ($\partial T_N/\partial \Delta_N = 0$) decreased when the loading angle increased (Figures 4 and 6). Although loaded in different directions, the normal stiffness ($\partial T_N/\partial \Delta_N$) remained constant (Figures 4 and 6). On the other hand, the tangential stiffness ($\partial T_T/\partial \Delta_T$) was found to increase as a function of the loading angle.

For model 2, addition of an extra bone and cement layer did not affect the response in pure tension (0°) (Figure 8(a)). On the other hand, in pure shear (90°), the extra layers (ELs) made the response in the tangential direction more compliant (Figure 8(b)); the tangential stiffness ($\partial T_T/\partial \Delta_T$) decreased from 241 to 167 MPa/mm. However, when the same gage length in the extended model 2 was considered as in the original model, the difference in mechanical response was negligible. In contrast to the aforementioned phenomena, the coupled stiffness ($\partial T_N/\partial \Delta_T$) based on the original gage length of the extended model did not match the ($\partial T_N/\partial \Delta_T$) response of the original model 2 (Figure 8(b)). Considering an equal applied load, the extended model resulted in the largest tangential deformation (Figure 8(c)). Again when considering the same gage length in the extended model as the original model 2, the deformations were nearly identical.

Finally, the relation between the mechanical response and the morphology was investigated. The maximum tensile traction (T_N) that occurred under tensile loading ($\partial T_N/\partial \Delta_N = 0$) was found to be moderately correlated with the average normal interdigitation ($int_{N,\alpha}$) ($r^2 = 0.54$; Figure 9(a)). Different loading directions did not strongly influence the normal stiffness ($\partial T_N/\partial \Delta_N$) in tension and compression (Figures 4 and 6) and could, therefore, not be related to the average normal interdigitation ($int_{N,\alpha}$) ($r^2 = 0.00002$ and $r^2 = 0.21$ for tension and compression, respectively; Figure 9(b)). The tangent stiffness at different load angles ($\partial T_T/\partial \Delta_T$) showed no

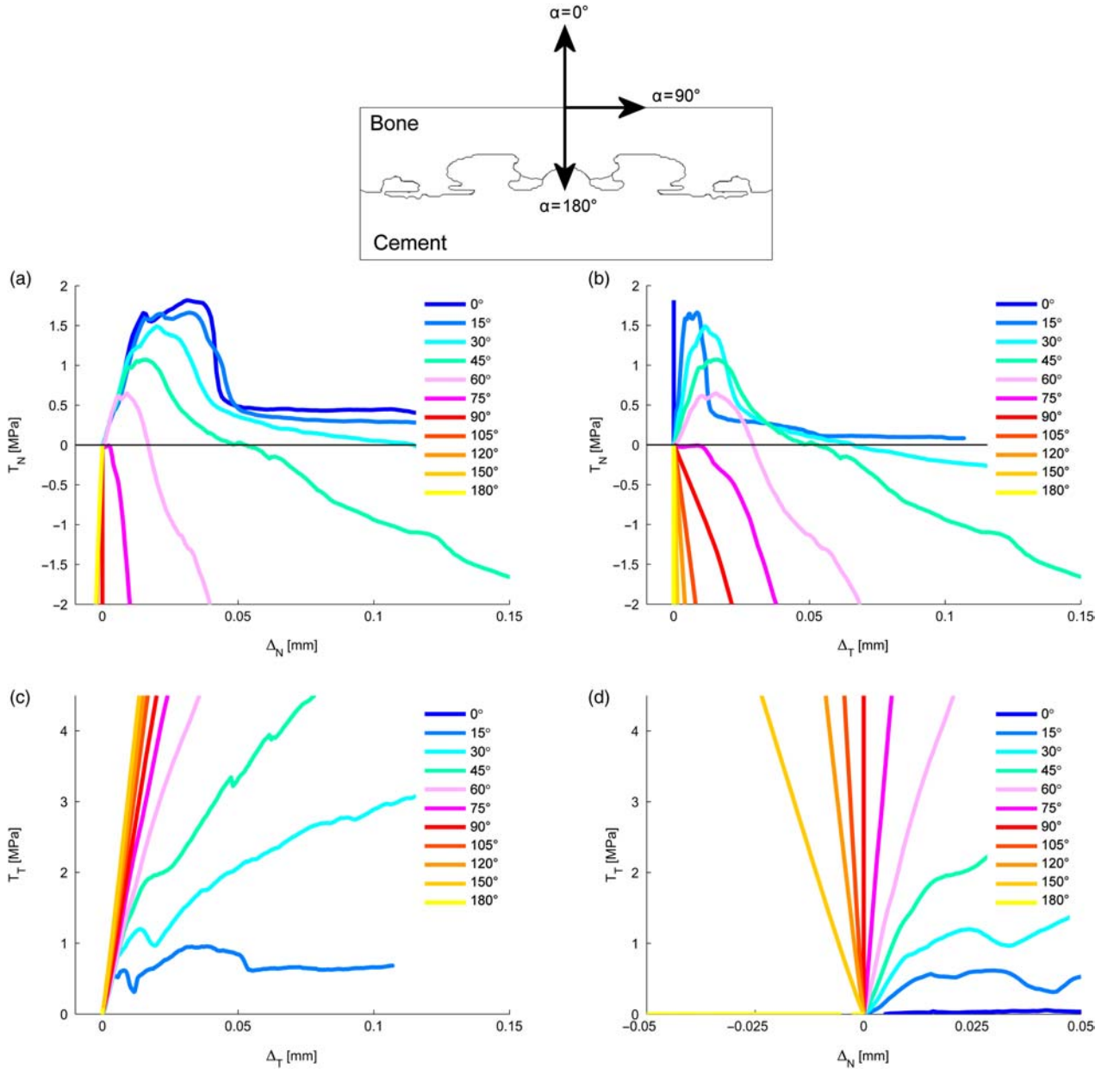

Figure 4. The traction–displacement relationships between T_N and Δ_N (a), T_N and ΔT (b), T_T and Δ_T (c) and T_T and Δ_N (d) of model 1 for 11 different angles. In pure tension ($\alpha = 0°$), the complete traction–displacement response is captured in subfigure (a). Obviously, no Δ_T took place in pure tension (b) and as a result of the symmetry no T_T occurred (d). In pure compression ($\alpha = 180°$), there was a very stiff $T_N - \Delta_N$ response (a), again without any Δ_T (b) and T_T (d). In pure shear ($\alpha = 90°$), no ultimate strength was found (c) and a considerable T_N was needed to prevent dilation of the bone (b). The mixed-mode responses showed a gradual decrease in ultimate T_N as the loading angle increased.

correlation with the average tangential interdigitation ($\text{int}_{T,\alpha}$) ($r^2 = 0.03$; Figure 9(c)).

Discussion

In this study, four generalised plain strain FEA models were used to investigate the mixed-mode response of the cement–bone interface. The analysis represented a basis for the implementation of an *ad hoc* cohesive law.

The results show that the ultimate tensile strength ($T_{N,ult}$) and stiffness ($\partial T_N/\partial \Delta_N$) determined for each model compare well with experimental observations, while the compressive stiffness is overestimated (Table 1). The response in shear also results in a satisfactory stiffness ($\partial T_T/\partial \Delta_T$) relative to experimental findings, but differs from the simulated tensile response as no ultimate strength is found. This can be explained by the crack patterns,

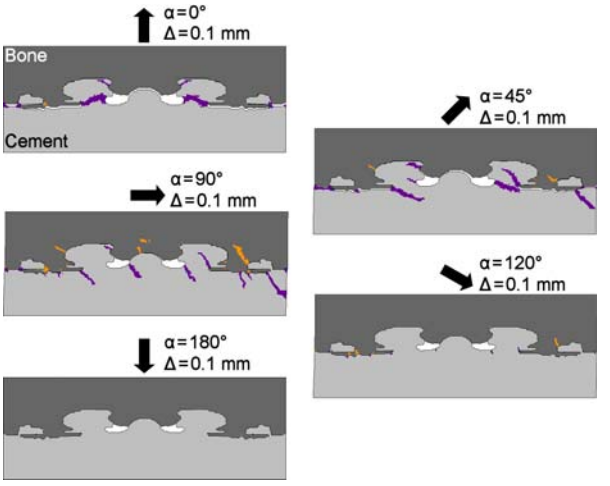

Figure 5. Crack patterns in the cement (purple) and bone (orange) of model 1 after $\Delta = 0.1$ mm displacement under five different load angles. At $\alpha = 0°$, the cement spurs were completely destructed, what resulted in almost no T_N (Figure 4(a)). At $\alpha = 90°$, however, cracks travelled into the bulk of the bone and cement instead of breaking off spurs, what resulted in no ultimate strength in shear (Figure 4(c)). The crack patterns that arose at $\alpha = 45°$ showed a combination of the crack patterns in pure tension and shear. In pure compression ($\alpha = 180°$), hardly any cracks occurred.

which show that bone and cement spurs break off in tension, while in shear the cracks progress into the bulk materials. Additionally, a considerable compressive traction is needed to prevent dilation of the interface. All mixed-mode responses show a gradual transition between the three 'principal' responses: tension, shear and compression.

The mechanical mixed-mode response cannot be related to the interface morphology in terms of cement interdigitation. The ultimate strength in normal direction for all the mixed modes and the normal and tangential stiffness showed either a poor or no correlation with the average normal and tangential interdigitation of the cement.

In the original models, the top edge of the bone and bottom edge of the cement were modelled with an ~1 mm offset relative to the contact interface to avoid mechanical boundary artefacts such as stress concentration and crack progression. To study the influence of such boundary conditions, the offset of model 2 was extended by adding an extra cement and bone layer. This EL appears not to affect the normal response, but makes the tangential response more compliant. However, when the same gage length as the original model 2 is considered, the response matches the response of the original model 2. This indicates that in the shear direction, extending the boundary conditions does not have an effect on the near interface deformation field. However, the addition of the ELs increases the compliance in the axial direction, which in turn reduces the amount of compression generated during shear loading. One would anticipate that additional extension of the cement and bone offset would further reduce the coupled stiffness, $(\partial T_N/\partial \Delta_T)$.

When loaded in pure tension (0°), fully symmetric crack patterns arise in the cement–bone interface as a result of the symmetric morphology (Figure 5). In pure shear (90°), the cracks progress into the bulk material. This type of cracking at the cement–bone interface was reported before (Yang et al. 2010). The crack patterns that occur when loaded in 45° tend to be a combination of the crack patterns in 0° and 90°; spurs break off and cracks progress into the bulk (Figure 5).

In pure shear, a considerable compressive traction is generated which prevents dilation of the interface. Moreover, no ultimate strength was found in pure shear, which is different from experimental findings. This can be explained by the experimental set-up used in these tests in which linear sliders were used, which result in no interfacial normal stresses when loaded in shear (Mann et al. 1999, 2001; Kim et al. 2004). This allows the interface to open (Lee et al. 2001), but is neglected in the overall motion analysis (Mann et al. 2009), in contrast to the current study. However, recently, shear experiments of the cement–bone interface have been performed in which the interface was not allowed to dilate (Yang et al. 2010). In this study, ultimate shear strengths were found which exceeded 20 MPa; considerably larger compared to the studies in which interfacial dilation was allowed. FEA studies on other interfaces have demonstrated that normal compression stresses do occur in pure shear

Table 1. Morphological and mechanical parameters of the four models and experiments (Mann et al. 2008; Waanders et al. 2010), while the ultimate tensile strength, $T_{N,ult}$ and the stiffness at 0° and 90° fell in the range with what has been found previously, the compressive stiffness was over-predicted.

Model	int_N (mm)	int_T (mm)	$0°T_{N,ult}$ (MPa)	$0°(\partial T_N/\partial \Delta_N)$ (MPa/mm)	$180°(\partial T_N/\partial \Delta_N)$ (MPa/mm)	$90°(\partial T_T/\partial \Delta_T)$ (MPa/mm)
1	0.21	5.84	1.82	123	888	217
2	0.26	5.14	2.79	251	975	241
3	0.03	3.08	1.28	149	769	294
4	0.48	4.36	2.19	172	1538	323
Experimental	0.14–0.48	No data	1.2–6.4	61.7–587	84–630	25.3–301

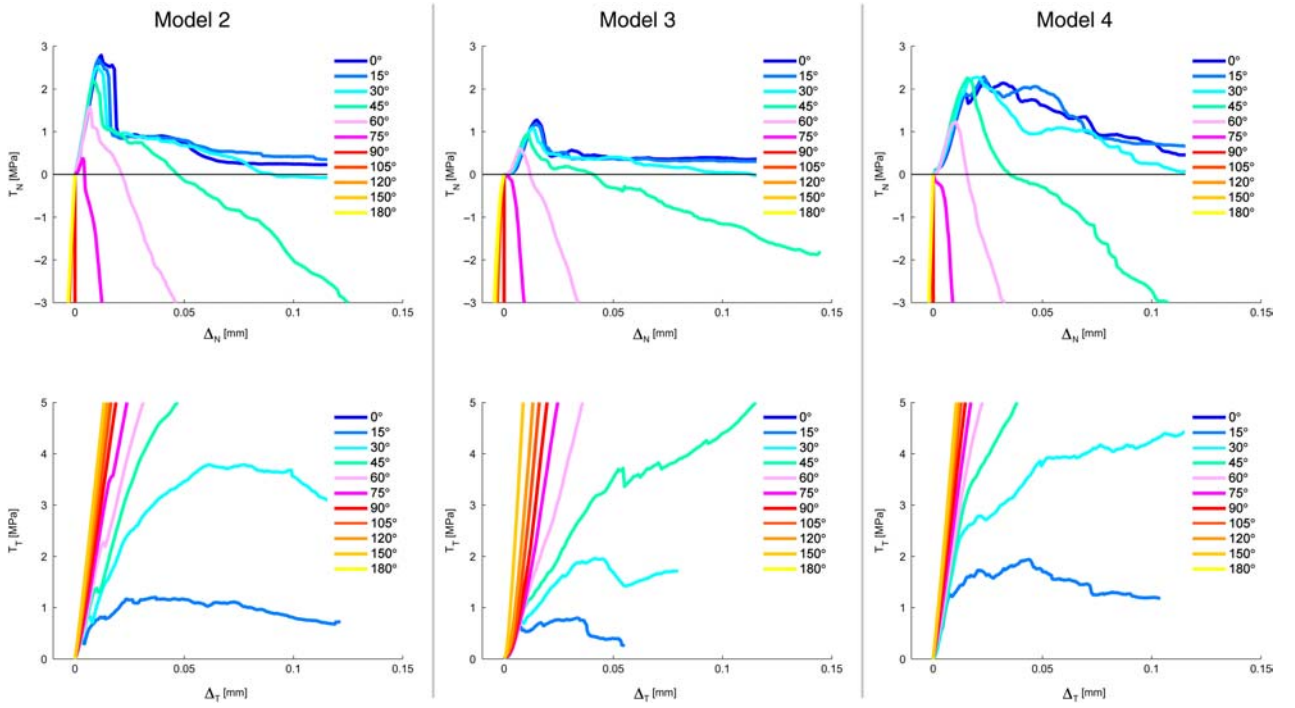

Figure 6. The $T_N - \Delta_N$ and $T_T - \Delta_T$ relationships for the models 2–4. The mixed-mode responses of model 1 was already shown in Figure 4. In pure tension, the models 2 and 3 resulted in a rather 'brittle' response, while model 4 was more ductile.

loading of interfaces (Salomonsson 2008). It is believed that this is caused by the formation of micro cracks and shear hackles in the interlaced interface (Pettersson et al. 2006). These features were also found in the current study (Figures 5 and 7).

By means of the implementation of periodic boundary conditions, one cement–bone interface model represents the complete cement–bone interface of a complete hip reconstruction. The periodic boundary conditions are applied using links, which provide equal displacements on both sides of the model (Salomonsson and Andersson 2008). The initial mirroring of the models consequently results in bone-to-bone and cement-to-cement links. The results show that the periodic boundary conditions result in stress distributions that are smoothly transferred from the model's left side to its right side (Figure 7). Also, cracks that progressed into one of the model's sides continued progressing out of the opposite side (Figure 7) indicating that the boundary conditions functioned properly.

Our study limitations include the modelling of the cement–bone interface, which was considered as 2D plain strain models instead of complete 3D models of the interface. Although the plane strain models result in satisfactorily ultimate tensile strengths, the accompanying displacement at peak strength is rather low compared to the experimental findings (Mann et al. 2008). Whether this 'brittle response' could be ascribed to the fact that 2D models were used is not clear, but 2D models do prohibit local motions in the third degree of freedom, which could contribute to more interfacial friction. Furthermore, the models are very stiff in compression, which could be attributed to the absence of significant gaps and cavities at the interface. Moreover, the applied periodic boundary conditions prohibit the models to expand as a result of the compression.

During the generation of the models used in this study, the models were mirrored. Although this does not represent a cement–bone interface portion that would occur *in vivo*, utilising symmetric models is commonly used in orthopaedic related FEA studies to apply the preferred boundary conditions (Mullins et al. 2007; Pahr and Zysset 2008; Kadir et al. 2010). Moreover, besides the boundary condition issue, mirroring is necessary to achieve the desired mechanical response. When the models have not been mirrored, confounding tangential tractions would occur when loaded in pure tension.

To relate the mechanical mixed-mode response of the cement–bone interface to interface morphology, we have focused on the cement penetration into the bone, which has not been proven to be a reliable parameter for mechanical comparisons in tension and shear (Waanders et al. 2010). Other approaches such as the quantitative CT-density and the contact area between the bone and cement were not used, since these 'global' parameters could not be converted to a directional dependent value. To determine the angular-dependent cement penetration, we have used

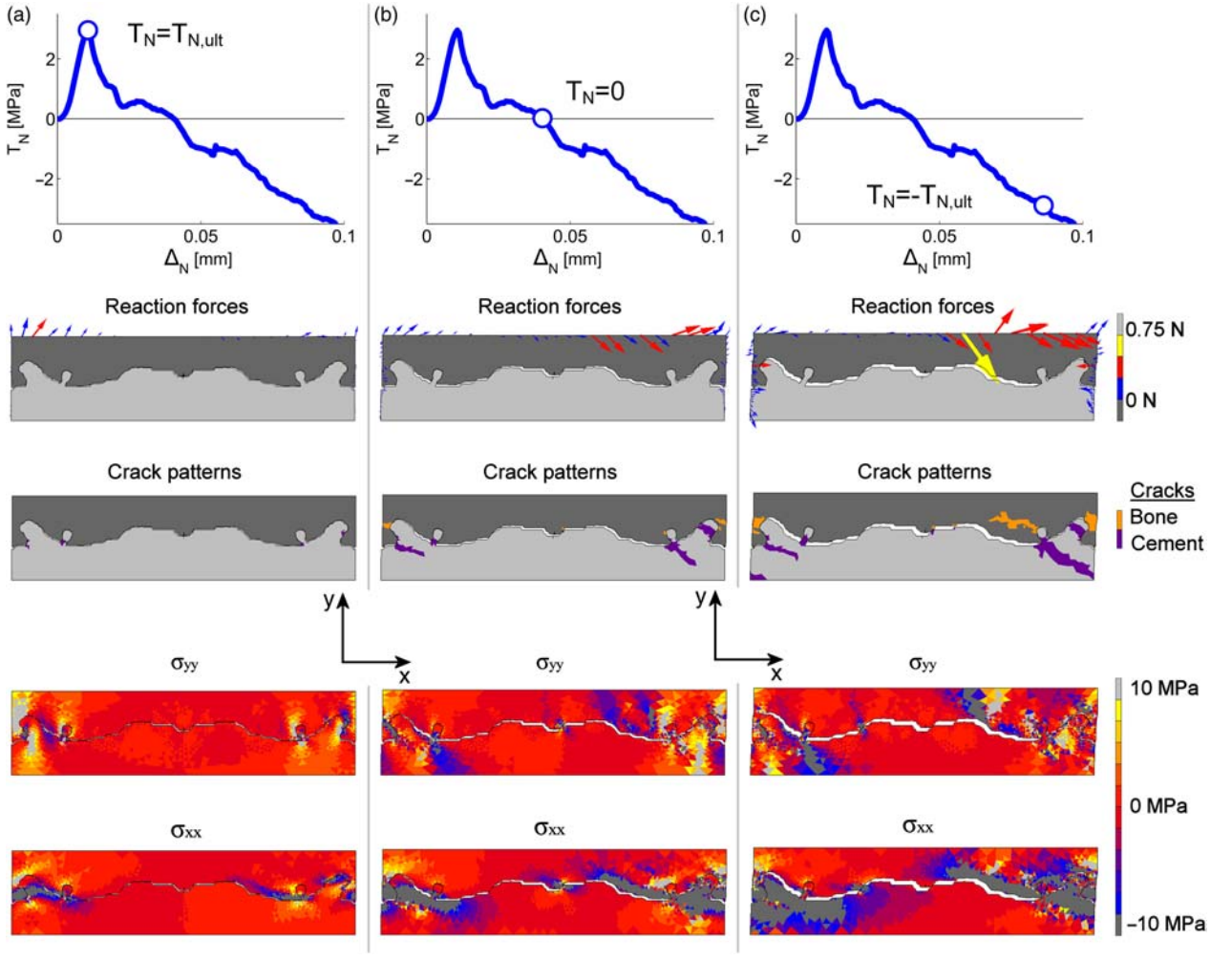

Figure 7. Post-failure response of model 3 when loaded at 45°. Bone reaction forces, crack patterns and stress fields, σ_{xx} and σ_{yy}, at three different moments during the failure response: (a) $T_N = T_{N,ult}$, (b) $T_N = 0$ and (c) $T_N = -T_{N,ult}$. The crack patterns at $T_N = -T_{N,ult}$ show bone and cement cracks that enter the model's right-hand side and continue progressing from the left side as a result of the periodic boundary conditions.

an approach that used the maximum normal and tangential cement penetration as a function of the loading angle. Quantifying the cement penetration for each loading angle would result in measurement difficulties, due to the differences in grid distances and the interfacial with over which the grid is spanned.

Another limitation of our study is that the effect of damage occurring under a certain load/direction on the mechanical response in another direction have been investigated. For example, it is not known how a complete fracture, as a result of a pure tensile load, affects the mechanical response in tangential direction with respect to the undamaged tangential response. Additional simulations could be performed in which for each loading angle, multiple damage stages are captured. Subsequently, these damaged cases would be loaded in other directions. However, this fell beyond the scope of the current study.

A similar limitation is the path dependency, which was not investigated. In this study, the top plane of the bone is consequently moved in one direction starting from the origin. Other paths, such as a normal displacement followed by a tangential displacement, were not considered. However, it was previously shown that the loading path has significant influence on the mechanical response (van den Bosch et al. 2006; Park et al. 2009).

The results show that the cement–bone interface is almost infinitely strong in pure shear. However, experimental tests have shown that this is not the case (Mann et al. 1999, 2001; Yang et al. 2010). The discrepancy between these two findings can be explained by the rigid boundary conditions that were applied to our micro-model, which are absent in reality. For example, the simulations do not allow any movement in normal direction if a pure shear was applied. In reality, the surrounding material will

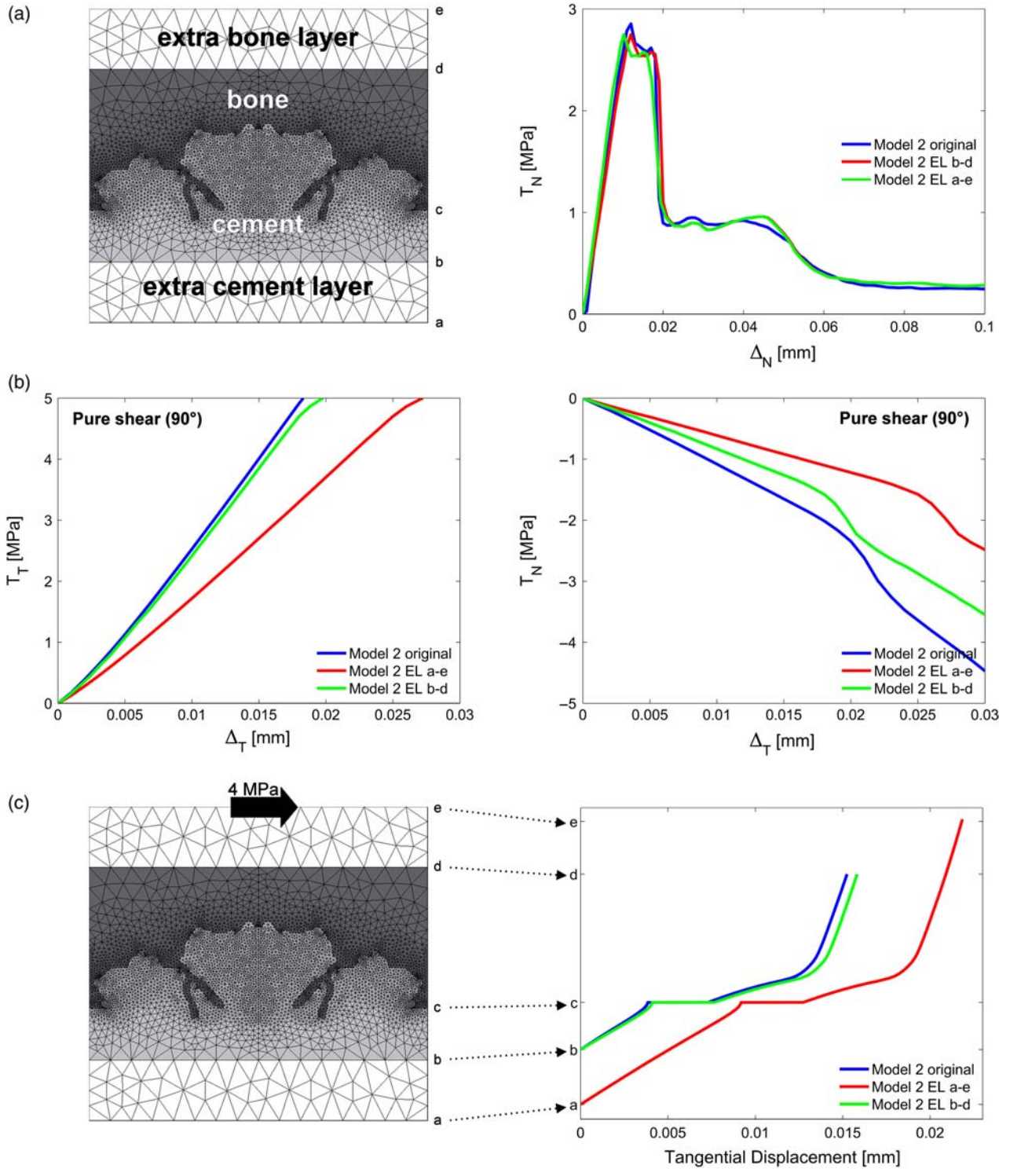

Figure 8. (a) There was negligible difference in tensile response (0°) between the original model 2 and the extended model 2 with 1 mm EL of bone and cement. (b) When loaded under 90° angle, the response of the extended model 2 was more compliant in the tangential as well as the normal direction. The tangential stiffness ($\partial T_T/\partial \Delta_T$) decreased from 241 to 167 MPa/mm. However, considering the same area as the original model 2, there was hardly any difference in tangential stiffness. (c) When loaded with 4 MPa in tangential direction, there were only some small differences in tangential displacement between the original model 2 and the same area of the extended model 2. The extended model 2 resulted in more tangential displacement.

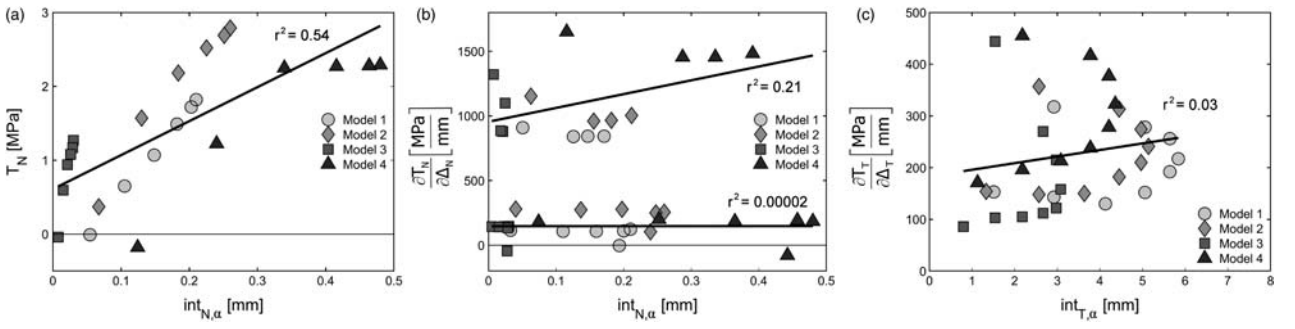

Figure 9. (a) Relationship between the maximum tensile traction, T_N and the average normal interdigitation, $int_{N,\alpha}$, ($r^2 = 0.54$). (b) Relationship between the normal stiffness, ($\partial T_N/\partial \Delta_N$) and the average normal interdigitation, $int_{N,\alpha}$, resulted in no correlation in tension ($r^2 = 0.00002$) and a poor correlation in compression ($r^2 = 0.21$). (c) Relationship between the tangential stiffness, ($\partial T_T/\partial \Delta_T$) and the average tangential interdigitation, $int_{T,\alpha}$, ($r^2 = 0.03$).

be compliant and allow deformation in normal direction. Therefore, the information obtained with the micro-models in this study should be considered as describing the mechanical behaviour of the cement–bone interface layer itself. If this behaviour is implemented around cemented total joint reconstructions, the compliance of the surrounding material will govern the external boundary conditions. This will allow the interface to dilate and fail at realistic shear strength values.

The goal of this study was to generate data on the mixed-mode response of the cement–bone interface for implementation in cohesive elements. Cohesive models that were developed in the past might not be applicable for the response found in this study, because these models assume separate fracture energies in tension and shear (Xu and Needleman 1993; Alfano and Crisfield 2001; Park et al. 2009). Our study, however, does not find a consistent value for the fracture energy in shear, because no failure is predicted. A possible solution is to include a cohesive model in which a global fracture energy is used instead of two separate fracture energies and the possibility to define an interface specific mechanical response in pure shear (Wei and Hutchinson 2008). Besides the numerical implementation of cohesive failure models into cohesive elements, it is also important to emphasise the physical implementation of the cohesive element into the mesh. This study demonstrated that the offset of the top and bottom edge relative to the contact area influences the shear properties of that specific portion of the cement–bone interface (Figure 8). Therefore, one should be aware that when implementing the reported mechanical response in complete models of cemented hip reconstructions, the cohesive element not only captures the interface, but also some adjacent material.

In conclusion: (1) this study revealed novel features of the cement–bone interface such as considerable compressive tractions and no failure in shear. The predicted tensile strength and stiffness and the shear stiffness positively match with previous experimental findings and (2) the mechanical response could not be related to the interfacial morphology in terms of cement penetration. Overall, we conclude that this study exhibited enough detail of the mechanical mixed-mode response of the cement–bone interface for implementation in cohesive elements.

Acknowledgements

This work was funded by the NIH grant AR42017.

Notes

1. Email: d.janssen@orthop.umcn.nl
2. Email: bertoldi@seas.harvard.edu
3. Email: k.bertoldi@utwente.nl
4. Email: mannk@upstate.edu
5. Email: n.verdonschot@orthop.umcn.nl
6. Email: n.verdonschot@utwente.nl

References

Alfano G, Crisfield MA. 2001. Finite element interface models for the delamination analysis of laminated composites: mechanical and computational issues. Int J Numer Methods Eng. 50:1701–1736.

Bishop NE, Schoenwald M, Schultz P, Puschel K, Morlock MM. 2009. The condition of the cement mantle in femoral hip prosthesis implantations – a post mortem retrieval study. Hip Int. 19:87–95.

Colombi P. 2002. Fatigue analysis of cemented hip prosthesis: model definition and damage evolution algorithms. Int J Fatigue. 24:895–901.

Harper EJ, Bonfield W. 2000. Tensile characteristics of ten commercial acrylic bone cements. J Biomed Mater Res. 53: 605–616.

Hung JP, Chen JH, Chiang HL, Wu JS. 2004. Computer simulation on fatigue behavior of cemented hip prostheses: a physiological model. Comput Methods Programs Biomed. 76:103–113.

Janssen D, Mann KA, Verdonschot N. 2008. Micro-mechanical modeling of the cement–bone interface: the effect of friction, morphology and material properties on the micromechanical response. J Biomech. 41:3158–3163.

Janssen D, Mann KA, Verdonschot N. 2009. Finite element simulation of cement–bone interface micromechanics: a comparison to experimental results. J Orthop Res. 27: 1312–1318.

Kadir MR, Syahrom A, Ochsner A. 2010. Finite element analysis of idealised unit cell cancellous structure based on morphological indices of cancellous bone. Med Biol Eng Comput. 48(5):497–505.

Katoozian H, Davy DT. 2000. Effects of loading conditions and objective function on three-dimensional shape optimization of femoral components of hip endoprostheses. Med Eng Phys. 22:243–251.

Keyak JH, Kaneko TS, Tehranzadeh J, Skinner HB. 2005. Predicting proximal femoral strength using structural engineering models. Clin Orthop Relat Res. 437:219–228.

Kim DG, Miller MA, Mann KA. 2004. A fatigue damage model for the cement–bone interface. J Biomech. 37:1505–1512.

Lee HS, Park YJ, Cho TF, You KH. 2001. Influence of asperity degradation on the mechanical behavior of rough rock joints under cyclic shear loading. Int J Rock Mech Min Sci. 38: 967–980.

Lewis G. 1997. Properties of acrylic bone cement: state of the art review. J Biomed Mater Res. 38:155–182.

Lewis G, Duggineni R. 2006. Finite element analysis of a three-dimensional model of a proximal femur-cemented femoral THJR component construct: influence of assigned interface conditions on strain energy density. Bio-Med Mater Eng. 16:319–327.

Lotz JC, Gerhart TN, Hayes WC. 1991. Mechanical properties of metaphyseal bone in the proximal femur. J Biomech. 24: 317–329.

Mann KA, Ayers DC, Werner FW, Nicoletta RJ, Fortino MD. 1997. Tensile strength of the cement–bone interface depends on the amount of bone interdigitated with PMMA cement. J Biomech. 30:339–346.

Mann KA, Damron LA. 2002. Predicting the failure response of cement–bone constructs using a non-linear fracture mechanics approach. J Biomech Eng. 124:462–470.

Mann KA, Miller MA, Cleary RJ, Janssen D, Verdonschot N. 2008. Experimental micromechanics of the cement–bone interface. J Orthop Res. 26:872–879.

Mann KA, Miller MA, Race A, Verdonschot N. 2009. Shear fatigue micromechanics of the cement–bone interface: an *in vitro* study using digital image correlation techniques. J Orthop Res. 27:340–346.

Mann KA, Mocarski R, Damron LA, Allen MJ, Ayers DC. 2001. Mixed-mode failure response of the cement–bone interface. J Orthop Res. 19:1153–1161.

Mann KA, Werner FW, Ayers DC. 1999. Mechanical strength of the cement–bone interface is greater in shear than in tension. J Biomech. 32:1251–1254.

Miller MA, Eberhardt AW, Cleary RJ, Verdonschot N, Mann KA. 2010. Micromechanics of postmortem-retrieved cement–bone interfaces. J Orthop Res. 28:170–177.

Moreo P, Garcia-Aznar JM, Doblare M. 2007. A coupled viscoplastic rate-dependent damage model for the simulation of fatigue failure of cement–bone interfaces. Int J Plast. 23: 2058–2084.

Moreo P, Perez MA, Garcia-Amar JM, Doblare M. 2006. Modelling the mixed-mode failure of cement–bone interfaces. Eng Fract Mech. 73:1379–1395.

Mullins LP, McGarry JP, Bruzzi MS, McHugh PE. 2007. Micromechanical modelling of cortical bone. Comput Methods Biomech Biomed Engin. 10:159–169.

Pahr DH, Zysset PK. 2008. Influence of boundary conditions on computed apparent elastic properties of cancellous bone. Biomech Model Mechanobiol. 7:463–476.

Park K, Paulino GH, Roesler JR. 2009. A unified potential-based cohesive model of mixed-mode fracture. J Mech Phys Solids. 57:891–908.

Perez MA, Garcia-Aznar JM, Doblare M. 2009. Does increased bone–cement interface strength have negative consequences for bulk cement integrity? A finite element study. Ann Biomed Eng. 37:454–466.

Pettersson KB, Neumeister JM, Gamstedt EK, Oberg H. 2006. Stiffness reduction, creep, and irreversible strains in fiber composites tested in repeated interlaminar shear. Compos Struct. 76:151–161.

Race A, Miller MA, Mann KA. 2010. Novel methods to study functional loading micromechanics at the stem-cement and cement–bone interface in cemented femoral hip replacements. J Biomech. 43:788–791.

Salomonsson K. 2008. Mixed mode modeling of a thin adhesive layer using a meso-mechanical model. Mech Mater. 40: 665–672.

Salomonsson K, Andersson T. 2008. Modeling and parameter calibration of an adhesive layer at the meso level. Mech Mater. 40:48–65.

Stolk J, Janssen D, Huiskes R, Verdonschot N. 2007. Finite element-based preclinical testing of cemented total hip implants. Clin Orthop Relat Res. 456:138–147.

Stolk J, Verdonschot N, Murphy BP, Prendergast PJ, Huiskes R. 2004. Finite element simulation of anisotropic damage accumulation and creep in acrylic bone cement. Eng Fract Mech. 71:513–528.

van den Bosch MJ, Schreurs PJG, Geers MGD. 2006. An improved description of the exponential Xu and Needleman cohesive zone law for mixed-mode decohesion. Eng Fract Mech. 73:1220–1234.

Verdonschot N, Huiskes R. 1997. The effects of cement-stem debonding in THA on the long-term failure probability of cement. J Biomech. 30:795–802.

Waanders D, Janssen D, Mann KA, Verdonschot N. 2010. The mechanical effects of different levels of cement penetration at the cement–bone interface. J Biomech. 43:1167–1175.

Waanders D, Janssen D, Miller MA, Mann KA, Verdonschot N. 2009. Fatigue creep damage at the cement–bone interface: an experimental and a micro-mechanical finite element study. J Biomech. 42:2513–2519.

Wang JY, Tozzi G, Chen J, Contal F, Lupton C, Tong J. 2010. Bone–cement interfacial behaviour under mixed mode loading conditions. J Mech Behav Biomed Mater. 3: 392–398.

Wei Y, Hutchinson JW. 2008. Toughness of Ni/Al2O3 interfaces as dependent on micron-scale plasticity and atomistic-scale separation. Philos Mag. 88:3841–3859.

Xu XP, Needleman A. 1993. Void nucleation by inclusions debonding in a crystal matrix. Model Simul Mater Sci Eng. 1:111–132.

Yang DT, Zhang D, Arola D. 2010. Fatigue of the bone/cement interface and loosening of total joint replacements. Int J Fatigue. 32(10):1639–1649.